$CsPbX_3/SiO_x$ (X=Cl, Br, I) Monoliths Prepared *via* a Novel Sol-gel Route Starting from Cs_4PbX_6 Nanocrystals

Sungwook Park,[†,Δ] Ngoc Mai An,[†,§,Δ] Guilherme Almeida,[†] Francisco Palazon,[‖] Davide Spirito,[†] Roman Krahne, Zhiya Dang,[†] Luca de Trizio[†] and Liberato Manna[†,*]

[†]Nanochemistry Department, Istituto Italiano di Tecnologia, Via Morego 30, 16163 Genova, Italy

[§]Dipartimento di Chimica e Chimica Industriale, Università degli Studi di Genova, Via Dodecaneso, 31, 16146, Genova, Italy

[‖]Instituto de Ciencia Molecular, ICMol, Universidad de Valencia, C/ Catedrático J. Beltrán 2, 46980 Paterna, Spain

KEYWORDS: $CsPbX_3$, nanocrystal, transformation, silica, sol-gel, lead halide perovskite, LED

ABSTRACT: We have developed a facile synthesis of nanocomposites based on $CsPbX_3$ nanocrystals (NCs) surrounded by a silica shell. The synthesis starts from colloidal Cs_4PbX_6 NCs: these are mixed with tetraethyl orthosilicate (TEOS) and are transformed into $CsPbX_3$ NCs during the sol-gel reaction. The overall reaction delivers $CsPbX_3$ NCs encased in a silica shell. Enhanced moisture and thermal stability in air were observed from the $CsPbX_3$ NCs/SiO_x composite powders. Also, when mixing $CsPbX_3/SiO_x$ samples with different anion (X) composition, no anion exchange processes were observed, an indication that the silica shell acts as a robust barrier surrounding the NCs. The composites are then used as down-converter phosphors on top of a blue light-emitting diode (LED), delivering nearly ideal white light emission with the Commission Internationale de l'Eclairage (CIE) color coordinates (0.32, 0.33).

INTRODUCTION

Lead halide perovskites (LHPs) of general chemical formula $APbX_3$ ($A = Cs^+$, $CH_3NH_3^+$, $CH(NH_2)_2^+$ and $X = Cl^-$, Br^-, I^-) are a class of gap-tunable semiconductors that have attracted considerable attention in the last few years for practical applications in optoelectronic devices.[1-3] In the nanocrystal (NC) form, these semiconducting systems exhibit high emission efficiencies and narrow emission widths, which are highly desirable for lighting and display applications.[4-7] Furthermore, LHP NCs can be processed by solution methods at temperatures below 100 °C, thus offering a considerable economic advantage with respect to conventional phosphors (rare-earth-doped oxides and nitrides require reaction temperatures as high as 1000 °C) typically employed in white light-emitting diodes (W-LEDs).[4, 7-11] The commercial application of LHPs is, however, hindered due to toxicity concerns (related to the presence of Pb) and poor ambient stability. At the NC scale, these issues can be mitigated by encapsulating or blending the NCs with other non-toxic materials.[12-26] For example, the encapsulation of LHP NCs with metal/metalloid oxide (MO) shells (e.g., TiO_x, SiO_x) has already been shown to improve both moisture and thermal stability.[27, 28] Moreover, the shelling suppresses undesirable phenomena such as merging of NCs or intra-NCs ion-exchange reactions, which lead to a change in their emission color.[6, 29, 30]

Among the various MOs, silicon oxide (SiO_x) emerges as a preferential encapsulation material due to its high optical transparency, chemical stability, abundance, non-toxicity, and low-cost.[31] SiO_x coated NCs have found applications in both biomedical[32] and optoelectronics fields.[33-35] While there are several different techniques to embed NC materials into silica matrixes,[36-39] the sol-gel route is the most employed one. In it, the silica shell is grown directly in solution from the decomposition of orthosilicates, such as tetraethyl orthosilicate (TEOS)[40] or tetramethyl orthosilicate (TMOS),[40-42] and this process can be catalyzed by protic acids, typically mineral acids, such as HNO_3.[43] However, LHP NCs are not compatible with these minerals acids as they readily dissolve in water. This effect is exacerbated by the fact that the sol-gel procedures reported so far for the encapsulation of LHPs in SiO_x do not employ any acid catalyst, thus resulting in a slow hydrolysis reaction that intensifies the degradation of the LHP NCs.[28, 40, 44] To overcome such an issue, here we propose an acid-catalyzed sol-gel method which delivers SiO_x coated $CsPbX_3$ NCs starting from Cs_4PbX_6 NCs. It has been recently shown that water can drive the transformation of Cs_4PbX_6 (0D) into $CsPbX_3$ (3D) NCs.[45] Motivated by these findings, we use an aqueous HNO_3 solution not only to produce 3D NCs starting from the corresponding 0D ones, but also to simultaneously trigger the hydrolysis of TEOS to grow a silica matrix surrounding the final NCs. Hence, we devised an acid-catalyzed sol-gel route that is capable of both inducing the complete 0D→3D NCs conversion and the concomitant gelation of the silica precursor, achieving a full embedment of 3D NCs into a SiO_x matrix (see Scheme 1). By tuning the halide composition of the starting 0D NCs, we could achieve control over the stoichiometry of the final $CsPbX_3$/silica composite samples, and, consequently, over their emission colors. We prepared three composite materials, namely $CsPb(Cl,Br)_3/SiO_x$ emitting in the blue (460 nm), $CsPbBr_3/SiO_x$ emitting in the green (510 nm), and Mn-doped $CsPb(I,Br)_3/SiO_x$ emitting in the red (645 nm). All of them featured improved stability against heat and humidity with respect to uncoated colloidal $CsPbX_3$ NCs. Furthermore, undesirable anion exchange reactions were prevented when intermixing $CsPbX_3/SiO_x$

samples with different anion compositions. Finally, we demonstrated that our composite materials could be used as down converter luminophores in a white light-emitting diode (W-LED) capable of generating a nearly ideal white light with Commission Internationale de l'Eclairage (CIE) color coordinates of (0.32, 0.33), and a correlated color temperature (CCT) of 6186 K.

Scheme 1. Sol-gel route for the production of $CsPbX_3/SiO_x$ composite monoliths starting from Cs_4PbX_6 NCs

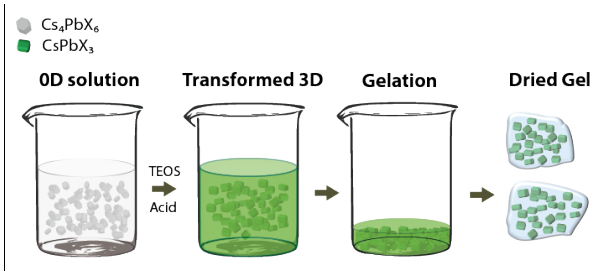

EXPERIMENTAL SECTION

Chemicals. Lead(II) chloride ($PbCl_2$, 99.999% trace metals basis), lead (II) bromide ($PbBr_2$, 99.999% trace metals basis), lead(II) iodide (PbI_2, 99.999% trace metals basis), cesium carbonate (Cs_2CO_3, reagent Plus, 99%), n-hexane (HEX, 99.5%), toluene (anhydrous, 99.5%), octadecene (ODE, technical grade, 90%), oleylamine (OLAM, 70%), oleic acid (OA, 90%), nitric acid (HNO_3, puriss. p.a., ≥65% w/w), Manganese(II) acetate tetrahydrate ($(CH_3COO)_2Mn{\cdot}4H_2O$, 99.99% trace metals basis), lead(II) oxide (PbO, 99.999% trace metals basis) and Tetraethyl orthosilicate (TEOS, 99.999% trace metals basis) were purchased from Sigma-Aldrich. All chemicals were used without any further purification.

Synthesis of Cs_4PbX_6 NCs. The synthesis was performed following the procedure reported in our previous work.[46] Briefly, 0.1 mmol of PbX_2 was combined with 5 mL of ODE, 0.2 mL of OA and 1.5 mL of OLAM in a 20 mL vial, and the mixture was heated on a hotplate set at 150 °C. After the complete dissolution of the PbX_2 salt, the solution was cooled down to the desired reaction temperature, and 0.75 mL of a 0.3 M Cs-oleate solution in OA (obtained by dissolving 0.4 g of Cs_2CO_3 in 8 mL of OA at 150 °C) was swiftly injected. After 30 seconds, the mixture became turbid white and was quickly cooled down to room temperature (RT) by plunging the vial into a water bath. The NCs were separated by centrifugation (at 4500 rpm for 10 minutes) and redispersed in 3 mL of hexane. Further details are presented in Table 1.

Table 1. Experimental conditions for the preparation of 0D Cs_4PbX_6 NCs

Composition	$PbBr_2$ (mmol)	$PbCl_2$ (mmol)	PbI_2 (mmol)	Reaction temperature (°C)
Cs_4PbBr_6	0.1			80
$Cs_4Pb(Cl,Br)_6$	0.05	0.05		100
$Cs_4Pb(I,Br)_6$	0.02		0.08	80

Synthesis of $CsPbX_3/SiO_x$ composites. 1 mL of Cs_4PbX_6 NCs solution ([Pb] ≈ 5 mM), 2 mL of hexane, 0.5 mL of TEOS, 20 μL of OA and 10 μL of a 0.1 M lead oleate solution in OA (prepared by dissolving 22 mg of PbO in 1 mL of OA at 100 °C) were loaded into a 20 mL vial under stirring. The vial was placed on a hot plate and heated to 100 °C. At this point, 10 μL of an aqueous solution of HNO_3 (65% w/w) was injected into the vial, and the reaction was allowed to proceed at 100 °C for 30 minutes. Subsequently, the vial was moved onto a stirring plate at RT and was left there for 10 hours after which a gel was obtained. We note that the vials were kept uncapped during the whole procedure. The gel was washed with 2 mL of hexane and separated by centrifugation (twice), and finally dried in a vacuum oven at 40 °C for 2 hours yielding a flaky product. The flakes were then ground to powders in an agate mortar. The preparation of Mn-doped $CsPb(I,Br)_3/SiO_x$ samples was similar, but in these cases we employed $Cs_4Pb(I,Br)_6$ NCs together with 0.2 mL of TEOS and 3 μL of HNO_3 solution containing 0.1 M $Mn(ac)_2$.

Optical Measurements. The UV–vis absorption spectra were recorded using a Varian Cary 5000 UV–Vis-NIR spectrophotometer equipped with an integrating sphere. The PL spectra were measured on a Varian Cary Eclipse spectrophotometer using an excitation wavelength of 350 nm for all the samples. Samples were prepared by dispersing the composite powders in hexane followed by drop-casting onto a quartz substrate.

Transmission Electron Microscopy (TEM). Low-resolution TEM measurements were performed on a JEOL-1100 TEM operating at an acceleration voltage of 100 kV. High-resolution TEM (HRTEM), high angle annular dark-field scanning TEM (HAADF-STEM) and Energy-dispersive X-ray spectroscopy (EDS) measurements were carried out on a JEOL JEM-2200FS microscope equipped with a 200 kV field emission gun, a CEOS spherical aberration corrector for the objective lens and an in-column image filter (Ω-type), on which a Bruker Quantax 400 system with a 60 mm^2 XFlash 6 T silicon drift detector (SDD) is mounted. Samples were prepared by dispersing the composite powders in hexane followed by drop-casting onto carbon-coated copper grids.

X-ray Diffraction (XRD). XRD patterns were acquired on a PAN analytical Empyrean X-ray diffractometer, equipped with a 1.8 kW Cu Kα ceramic X-ray tube and a PIXcel3D 2 × 2 area detector, operating at 45 kV and 40 mA, under ambient conditions using parallel beam geometry and symmetric reflection mode. Samples were prepared by pressing the composite powders onto a quartz zero-diffraction single crystal substrate.

Fabrication and characterization of W-LED. Dry powders of red- and green-emitting $CsPbX_3/SiO_x$ composites were finely ground in a mortar together with polymethylmethacrylate (PMMA) beads. The resulting powder mixture was then pressed into a solid pellet of 16 mm in diameter and *ca.* 1-2 mm in height. The as-obtained phosphor pellet was placed on top of a commercial blue LED (Thorlabs LIU470A) with an emission peak at 460 nm. The resulting white light spectrum was measured inside a Hamamatsu C9920-03 spectrometer equipped with an integrating sphere. The luminance was assessed with a Minolta LS-110 Luminance Meter.

RESULTS AND DISCUSSION

The starting Cs_4PbBr_6 (0D) NCs, synthesized by a hot injection colloidal approach,[46] had an average size of 13 nm and a XRD pattern

matching that of bulk Cs_4PbBr_6 hexagonal phase (Figure 1a). These NCs are wide-bandgap semiconductors characterized by a narrow optical absorption peak at 315 nm as can be seen from their absorbance spectrum (left side of Figure 1b). The 0D NCs were then converted to SiO_x coated $CsPbBr_3$ powders via a sol-gel route. Briefly, reacting the 0D NCs with TEOS in the presence of HNO_3 yielded luminescent green gels that were then dried to flakes and ground to powders (Figure 1c). The resulting powder exhibited an absorption onset at 490 nm and a photoluminescence (PL) emission peaking at 510 nm with full with at half maximum (FWHM) of 23.8 nm (114 meV) (right side of Figure 1b). The XRD pattern of this powder was in good agreement with the bulk $CsPbBr_3$ perovskite structure, as can be seen in Figure 1a, with no reflections ascribable to the starting 0D phase, indicating a full 0D to 3D conversion. TEM micrographs, TEM-EDS elemental maps and HR-TEM analysis revealed that these powders consist of 7 nm NCs embedded in an amorphous silica matrix (Figure 1f-g and S1).

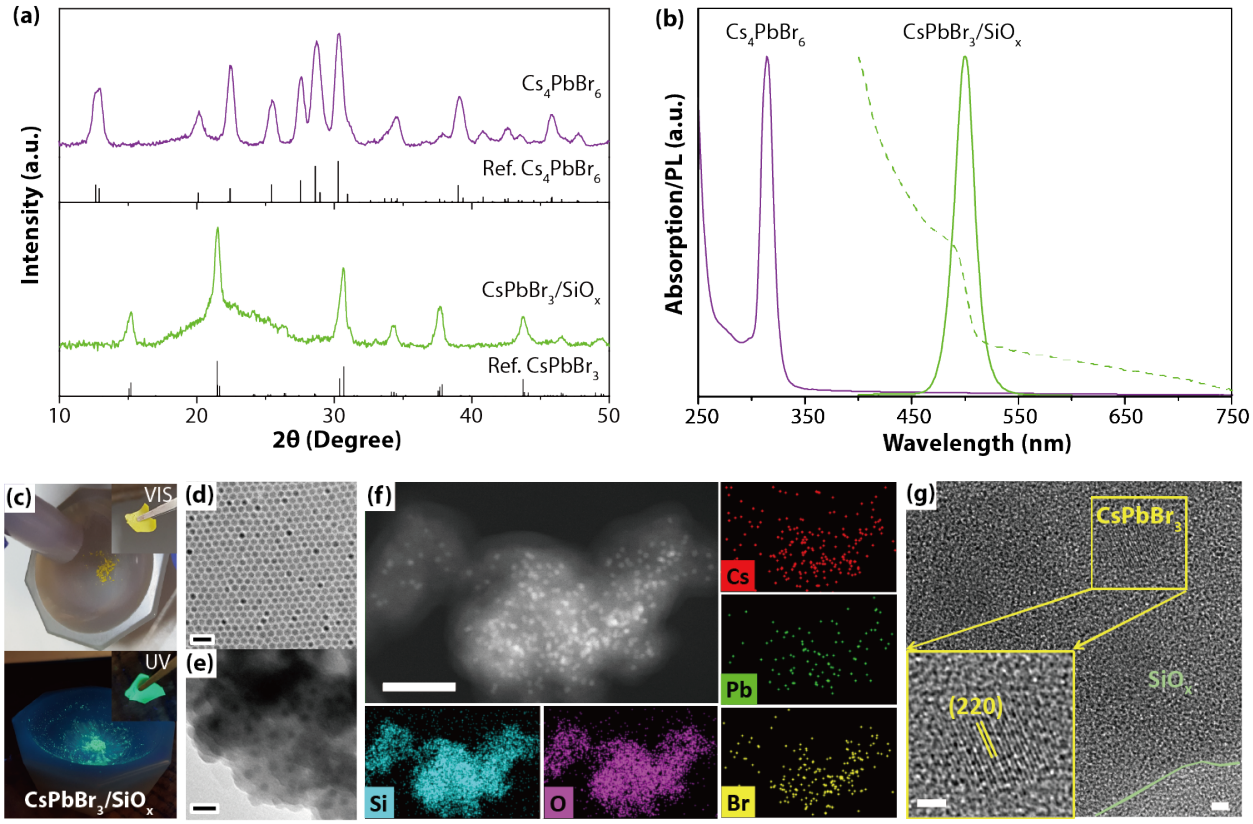

Figure 1. (a) XRD patterns of Cs_4PbBr_6 NCs (purple) and $CsPbBr_3/SiO_x$ composite (green) matching with the Cs_4PbBr_6 (ICSD 98-002-5124) and $CsPbBr_3$ (ICSD 98-009-7851) reference patterns, respectively; (b) Absorption spectrum of Cs_4PbBr_6 NCs (purple), and absorption and PL spectra of the $CsPbBr_3/SiO_x$ composite (green); (c) Photographs of the $CsPbBr_3/SiO_x$ composite powder under day light (upper panel) and 345 nm UV lamp (lower panel). The insets are the as-prepared flake; (d-e) TEM micrographs of (d) Cs_4PbX_6 NCs– scale bar is 40 nm, and (e) $CsPbBr_3/SiO_x$ composite– scale bars are 20 nm; (f) HAADF-STEM image and the corresponding elemental maps showing the distribution of Cs, Pb, Br, Si, O .Scale bar is 100 nm; (g) HRTEM image of a $CsPbBr_3$ NC embedded in an amorphous SiO_x matrix (inset is the magnified view of the particle) Scale bar is 2 nm.

Our sol-gel route can be described as a one-step approach in which two "main" reactions occur concomitantly:

i) the water-induced transformation of 0D to 3D NCs;[45]

$$Cs_4PbX_6 \xrightarrow{aq.HNO_3} CsPbX_3 + 3CsX \quad (1)$$

ii) the gelation of TEOS which is catalyzed by HNO_3:

$$Si(OC_2H_5)_4 + 4H_2O \Leftrightarrow Si(OH)_4 + 4\,C_2H_5OH \quad (2)$$

$$n\,Si(OC_2H_5)_4 + n\,Si(OH)_4 \Leftrightarrow (\text{-}SiO_2\text{-})_n + 4n\,C_2H_5OH \quad (3)$$

$$n\,Si(OH)_4 + n\,Si(OH)_4 \Leftrightarrow (\text{-}SiO_2\text{-})_n + 4n\,H_2O \quad (4)$$

Despite Eq. (1) implies the formation of CsX upon the 0D→3D transformation, the XRD pattern of our products did not evidence any crystalline by-products. However, in a control experiment we noted that in the absence of TEOS, the 3D phase was also obtained, but together with crystalline CsBr and $CsNO_3$ (see figure S3). These results suggested that the extracted CsX was not able to precipitate in a crystalline form during the sol-gel process (i.e. in the presence of TEOS). We also ran control experiments in which we employed 3D instead of 0D NCs in our sol-gel process. In these experiments, we observed the complete degradation of the NCs (Figure S4), an evidence of the better suitability of the "0D" Cs_4PbX_6 NCs in our sol-gel method. Hence, the strongly reactive environment is used at our advantage to convert in situ the 0D NCs to 3D $CsPbX_3$ NCs, while any further degradation reaction of the generated 3D NCs is quenched by the formation of the silica shell.

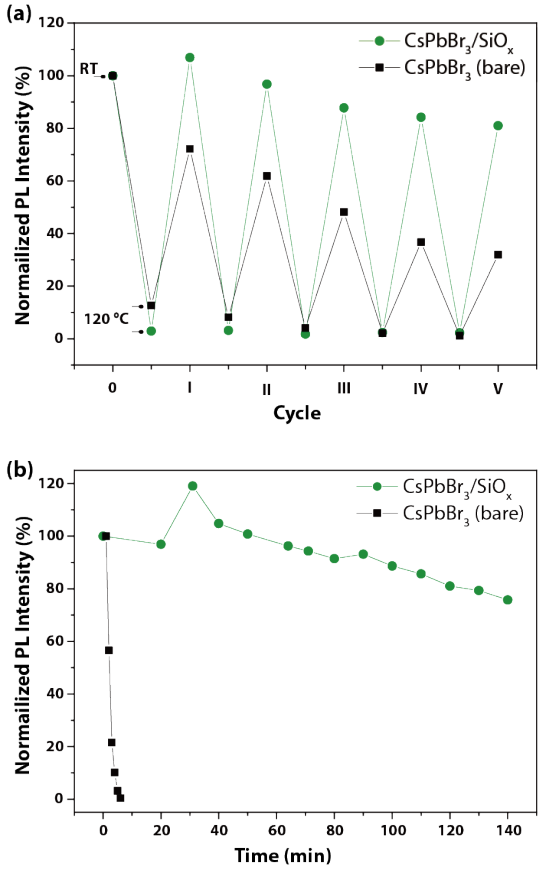

Figure 2. Thermal and water stability tests performed on both bare $CsPbBr_3$ NCs and $CsPbBr_3/SiO_x$ composite: (a) heating and cool down cycling measurements; (b) measured PL intensity changes of $CsPbBr_3$ and $CsPbBr_3/SiO_x$ were monitored during those were exposed to water under stirring, [Pb] ≈ 0.1 mM in both cases

After assessing the effective encapsulation of $CsPbBr_3$ NCs in the SiO_x matrix, we tested the stability of the $CsPbBr_3/SiOx$ composite against heat and water, and compared it with that of oleylamonium bromide coated $CsPbBr_3$ NCs prepared following the approach of Protesescu *et al.*,[47] and denoted here as "bare". The thermal stability was assessed by monitoring the photoluminescence (PL) of films during successive heating and cooling cycles (from room temperature -RT- to 120 °C, 1 hour/cycle). As shown in Figure 2a and S5, the PL of both samples was quenched upon increasing the temperature up to 120°C and then (partially) recovered upon cooling back to RT. After 5 cycles, the composite $CsPbBr_3/SiO_x$ sample retained 81% of the initial emission intensity while the PL of "bare" $CsPbBr_3$ NCs dropped to 31%. The stability against water was assessed by dispersing the samples in deionized (DI) water under stirring (Figure 2b) and monitoring the resulting PL. In detail, 2.3 mg of the $CsPbBr_3/SiO_x$ sample was dispersed in 3 mL DI water under stirring while monitoring the corresponding PL over time. As shown in figure 2b, after 140 minutes, the $CsPbBr_3/SiO_x$ sample retained 76% of the initial emission intensity, while the PL of bare $CsPbBr_3$ NCs was completely quenched within a few minutes. Our results indicate that SiO_x coating improves both the thermal and the water stability of the $CsPbBr_3$ NCs.

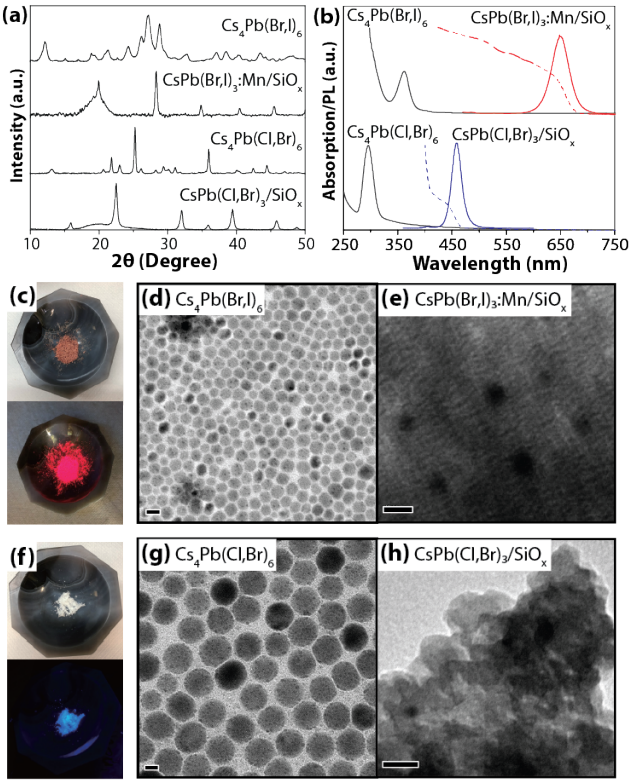

Figure 3. (a) XRD patterns of $Cs_4Pb(Br,I)_6$ and $Cs_4Pb(Cl,Br)_6$ NCs and $CsPb(Br,I)_3$:Mn/SiO_x and $CsPb(Cl,Br)_3/SiO_x$ composite powders; (b) Absorption of Cs_4PbX_6 NCs and absorption/PL spectra of $CsPbX_3/SiO_x$ composite powders; (c, f) Photographs of (c) $CsPb(Br,I)_3$:Mn/SiO_x and (f) $CsPb(Cl,Br)_3/SiO_x$ composite powders under daylight (upper panels) and under 345 nm UV lamp irradiation (lower panels). (d, e, g, h) The TEM image of the Cs_4PbX_6 NCs (d and g) and $CsPbX_3/SiO_x$ composite (e and h). Scale bars are 10 nm in all TEM images.

Motivated by these results, we decided to expand this procedure to the synthesis of blue- and red- emitting samples to be employed, together with the green emitting composite, in down converting W-LEDs. To do so, we applied our sol-gel route to mixed halide 0D samples, namely $Cs_4Pb(I,Br)_6$, and $Cs_4Pb(Cl,Br)_6$ NCs. The starting 0D NCs had a size of 16 nm for $Cs_4Pb(I,Br)_6$, and 22 nm for $Cs_4Pb(Cl,Br)_6$ and compositions (Figure 3d and g), as determined by SEM-EDS analysis, $Cs_4PbBr_{0.97}I_{5.03}$ and $Cs_4PbCl_{4.12}Br_{1.88}$, respectively (Figure S7-8). The XRD analysis of the sol-gel products, reported in Figure 3a, confirmed that 0D mixed halide NCs were converted into the corresponding 3D structures. TEM images show that 3D NCs are embedded in a silica matrix (Figure 3e and h). The resulting Mn-doped $CsPb(Br,I)_3/SiO_x$ powder was characterized by a bright PL emission at 645 nm with a FWHM of 39.6 nm (117 meV) while the $CsPb(Cl,Br)_3/SiO_x$ sample had a PL emission at 460 nm with a FWHM of 22.6 nm (133 meV) (Figure 3b). The emission colors of the samples can be seen in Figure 3c and f. We would like to mention here that a small amount of Mn^{2+} ions was employed in the sol-gel process involving $Cs_4Pb(I,Br)_6$ NCs with the aim of improve the stability of the resulting sample (see Experimental Section

for details).[48] In the absence of Mn^{2+} the process resulted in a non-luminescent material (see Figure S6).

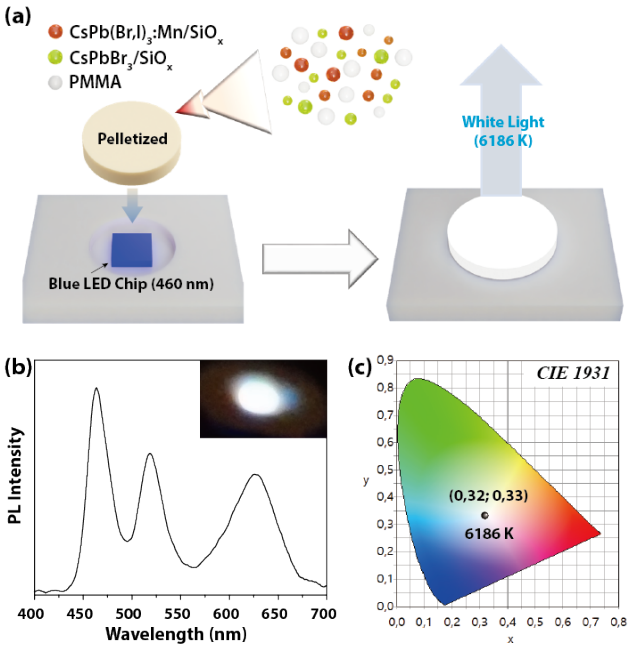

Figure 4. (a) Schematic structure of W-LED fabrication. Red and green $CsPbX_3/SiO_x$ composite powders are covered on the 460 nm blue LED. (b) The emission spectrum of the fabricated W-LED (inset: photograph of the W-LED under operation) (c) CIE1931 color coordinate diagram.

Our composite $CsPbX_3/SiO_x$ samples were finally employed as down-conversion phosphors on top of a blue commercial LED. In order to do this, green- and red-emitting $CsPbX_3/SiO_x$ powders were mixed with PMMA, finely ground and pressed into a solid pellet (see figure 4a for a schematic representation of the process and the experimental section for more details). The resulting emission spectrum is displayed in figure 4b, where the three peaks for the blue LED, and two different phosphors are visible. It is worth noting that green- and red-emitting phosphors maintained their color purity in the pellet, confirming that the different NCs are well separated and no unwanted anion-exchange reactions took place, which would otherwise have led to a single yellow emission.[49] As a result, the CIE coordinates of (0.32; 0.33), represented in figure 4c, we are very close to the ideal white coordinates (0.33; 0.33) and corresponded to a color-correlated temperature (CCT) of 6186 K, suitable for most lighting and display applications. In addition, the color-rendering index (CRI) was 69. Eventually, we measured the luminance of the commercial blue LED with and without the down-converting pellet finding values of 102 cd/m^2 and 29320 cd/m^2, respectively. The loss of luminance can be attributed to different factors, such as non-unity quantum yield of the phosphors and scattering losses in the relatively thick and rough pellet. Nonetheless, the value of 102 cd/m^2 is in the order of magnitude of most common PC and smartphone displays.

Conclusions

We have developed an easy and straightforward sol-gel procedure to produce different colors emitting $CsPbX_3$ NCs embedded in a SiO_x matrix. In such a process, we employed colloidal 0D Cs_4PbX_6 NCs that underwent a water induced transformation into the corresponding 3D $CsPbX_3$ NCs during the sol-gel process itself. The sol-gel route was based on the combined use of TEOS and an aqueous solution of nitric acid as a catalyst. We demonstrated that the resulting amorphous silica matrix effectively embedded $CsPbX_3$ NCs, conferring them higher water and thermal stability. Besides, it prevented undesirable anion exchange between different halide perovskite NCs. Red and green emitting samples, that is, Mn-doped $CsPb(Br,I)_3/SiO_x$ and $CsPbBr_3/SiO_x$, were combined with a blue LED to produce a down converting W-LED. The resulting emission corresponded to a white-light with near-ideal color coordinates and good color rendering index. The results obtained here provide an effective strategy for silica coating and improving the material stability of LHP NCs that can be potentially applied in the display and lighting fields.

ASSOCIATED CONTENT

Supporting Information.
Controlled experiment details, complementary HAADF-STEM images, HR-TEM images, EDS elemental mappings and FT-IR spectra.
The PL spectrum of samples in thermal stability test.

A brief statement in nonsentence format listing the contents of material supplied as Supporting Information should be included, ending with "This material is available free of charge via the Internet at http://pubs.acs.org." For instructions on what should be included in the Supporting Information as well as how to prepare this material for publication, refer to the journal's Instructions for Authors.

AUTHOR INFORMATION

Corresponding Author

* (Word Style "FA_Corresponding_Author_Footnote"). Give contact information for the author(s) to whom correspondence should be addressed.

PresentAddresses

†If an author's address is different than the one given in the affiliation line, this information may be included here.

Author Contributions

ΔSungwook Park and Ngoc Mai An contributed equally to this work

Funding Sources

Any funds used to support the research of the manuscript should be placed here (per journal style).

Notes

Any additional relevant notes should be placed here.

ACKNOWLEDGMENT

(Word Style "TD_Acknowledgments"). Generally the last paragraph of the paper is the place to acknowledge people (dedications), places, and financing (you may state grant numbers and sponsors here). Follow the journal's guidelines on what to include in the Acknowledgement section.

REFERENCES

Uncategorized References

1. Q. A. Akkerman, G. Rainò, M. V. Kovalenko and L. Manna, *Nature Materials*, 2018, **17**, 394-405.
2. A. Kojima, K. Teshima, Y. Shirai and T. Miyasaka, *Journal of the American Chemical Society*, 2009, **131**, 6050-6051.
3. M. Liu, M. B. Johnston and H. J. Snaith, *Nature*, 2013, **501**, 395.
4. F. Zhang, H. Zhong, C. Chen, X.-g. Wu, X. Hu, H. Huang, J. Han, B. Zou and Y. Dong, *ACS Nano*, 2015, **9**, 4533-4542.
5. F. Liu, Y. Zhang, C. Ding, S. Kobayashi, T. Izuishi, N. Nakazawa, T. Toyoda, T. Ohta, S. Hayase, T. Minemoto, K. Yoshino, S. Dai and Q. Shen, *ACS Nano*, 2017, **11**, 10373-10383.
6. Q. A. Akkerman, V. D'Innocenzo, S. Accornero, A. Scarpellini, A. Petrozza, M. Prato and L. Manna, *Journal of the American Chemical Society*, 2015, **137**, 10276-10281.
7. S. Ananthakumar and S. Moorthy Babu, *Synthetic Metals*, 2018, **246**, 64-95.
8. Q. Zhou, Z. Bai, W.-g. Lu, Y. Wang, B. Zou and H. Zhong, *Advanced Materials*, 2016, **28**, 9163-9168.
9. J. Zhou, F. Huang, H. Lin, Z. Lin, J. Xu and Y. Wang, *Journal of Materials Chemistry C*, 2016, **4**, 7601-7606.
10. S. Shionoya, W. M. Yen and H. Yamamoto, *Phosphor Handbook*, CRC Press, 2018.
11. H. Suzuki, C. S. Yoon, H. S. Won, J. H. Ryu, Y. G. Park and S. H. Kim, *Journal*, 2012.
12. M. Meyns, M. Perálvarez, A. Heuer-Jungemann, W. Hertog, M. Ibáñez, R. Nafria, A. Genç, J. Arbiol, M. V. Kovalenko and J. Carreras, *ACS applied materials & interfaces*, 2016, **8**, 19579-19586.
13. L. Xi, C. B. Boothroyd, T. Salim, S. Borghardt, Y. M. Lam and B. E. Kardynał, *Journal of Materials Chemistry C*, 2017, **5**, 7207-7214.
14. X. Li, Z. Xue, D. Luo, C. Huang, L. Liu, X. Qiao, C. Liu, Q. Song, C. Yan and Y. Li, *Science China Materials*, 2018, **61**, 363-370.
15. H. Wu, S. Wang, F. Cao, J. Zhou, Q. Wu, H. Wang, X. Li, L. Yin and X. Yang, *Chemistry of Materials*, 2019.
16. S. Yang, F. Zhang, J. Tai, Y. Li, Y. Yang, H. Wang, J. Zhang, Z. Xie, B. Xu and H. Zhong, *Nanoscale*, 2018, **10**, 5820-5826.
17. N. Ding, D. Zhou, X. Sun, W. Xu, H. Xu, G. Pan, D. Li, S. Zhang, B. Dong and H. Song, *Nanotechnology*, 2018, **29**, 345703.
18. H. Li, X. Zheng, Y. Liu, Z. Zhang and T. Jiang, *Nanoscale*, 2018, **10**, 1650-1659.
19. S. Muduli, P. Pandey, G. Devatha, R. Babar, D. C. Kothari, M. Kabir, P. P. Pillai and S. Ogale, *Angewandte Chemie International Edition*, 2018, **57**, 7682-7686.
20. H. Huang, J. Li, Y. Yi, J. Wang, Y. Kang, P. K. Chu, H. Ong and X.-F. Yu, *Chemical Communications*, 2018, **54**, 2365-2368.
21. J. S. Chen, T. L. Doane, M. Li, H. Zang, M. M. Maye and M. Cotlet, *Particle & Particle Systems Characterization*, 2018, **35**, 1700310.
22. T. Xuan, S. Lou, J. Huang, L. Cao, X. Yang, H. Li and J. Wang, *Nanoscale*, 2018, **10**, 9840-9844.
23. L. Xu, J. Li, T. Fang, Y. Zhao, S. Yuan, Y. Dong and J. Song, *Nanoscale Advances*, 2019, **1**, 980-988.
24. Y. Wang, D. Yu, Z. Wang, X. Li, X. Chen, V. Nalla, H. Zeng and H. Sun, *Small*, 2017, **13**, 1701587.
25. L. N. Quan, R. Quintero-Bermudez, O. Voznyy, G. Walters, A. Jain, J. Z. Fan, X. Zheng, Z. Yang and E. H. Sargent, *Advanced Materials*, 2017, **29**, 1605945.
26. Y.-M. Chen, Y. Zhou, Q. Zhao, J.-Y. Zhang, J.-P. Ma, T.-T. Xuan, S.-Q. Guo, Z.-J. Yong, J. Wang and Y. Kuroiwa, *ACS applied materials & interfaces*, 2018, **10**, 15905-15912.
27. Z.-J. Li, E. Hofman, J. Li, A. H. Davis, C.-H. Tung, L.-Z. Wu and W. Zheng, *Advanced Functional Materials*, 2018, **28**, 1704288.
28. Q. Zhong, M. Cao, H. Hu, D. Yang, M. Chen, P. Li, L. Wu and Q. Zhang, *ACS Nano*, 2018, **12**, 8579-8587.
29. Z. Liu, Y. Zhang, Y. Fan, Z. Chen, Z. Tang, J. Zhao, Y. Lv, J. Lin, X. Guo and J. Zhang, *ACS applied materials & interfaces*, 2018, **10**, 13053-13061.
30. H. Huang, B. Chen, Z. Wang, T. F. Hung, A. S. Susha, H. Zhong and A. L. Rogach, *Chemical Science*, 2016, **7**, 5699-5703.
31. G. A. Sotiriou, T. Sannomiya, A. Teleki, F. Krumeich, J. Vörös and S. E. Pratsinis, *Advanced Functional Materials*, 2010, **20**, 4250-4257.
32. J. Wen, K. Yang, F. Liu, H. Li, Y. Xu and S. Sun, *Chemical Society Reviews*, 2017, **46**, 6024-6045.
33. J. Ziegler, S. Xu, E. Kucur, F. Meister, M. Batentschuk, F. Gindele and T. Nann, *Advanced Materials*, 2008, **20**, 4068-4073.
34. R. Ghosh Chaudhuri and S. Paria, *Chemical reviews*, 2011, **112**, 2373-2433.
35. P. Mulvaney, L. Liz-Marzan, M. Giersig and T. Ung, *Journal of Materials Chemistry*, 2000, **10**, 1259-1270.
36. W. K. Choi, W. K. Chim, C. L. Heng, L. W. Teo, V. Ho, V. Ng, D. A. Antoniadis and E. A. Fitzgerald, *Applied Physics Letters*, 2002, **80**, 2014-2016.
37. F.-l. Zeng, M. Yang, J.-l. Qin, F. Teng, Y.-q. Wang, G.-x. Chen, D.-w. Wang and H.-s. Peng, *ACS applied materials & interfaces*, 2018, **10**, 42837-42843.
38. T. R. Sathe, A. Agrawal and S. Nie, *Analytical Chemistry*, 2006, **78**, 5627-5632.
39. J. Kim, J. E. Lee, J. Lee, J. H. Yu, B. C. Kim, K. An, Y. Hwang, C.-H. Shin, J.-G. Park, J. Kim and T. Hyeon, *Journal of the American Chemical Society*, 2006, **128**, 688-689.
40. S. Huang, Z. Li, L. Kong, N. Zhu, A. Shan and L. Li, *Journal of the American Chemical Society*, 2016, **138**, 5749-5752.
41. Q. Zhong, M. Cao, H. Hu, D. Yang, M. Chen, P. Li, L. Wu and Q. Zhang, *ACS nano*, 2018, **12**, 8579-8587.
42. F. Zhang, Z.-F. Shi, Z.-Z. Ma, Y. Li, S. Li, D. Wu, T.-T. Xu, X.-J. Li, C.-X. Shan and G.-T. Du, *Nanoscale*, 2018, **10**, 20131-20139.
43. H. Ishida and G. Kumar, *Molecular Characterization of Composite Interfaces*, Springer US, 1985.
44. R. Ciriminna, M. Sciortino, G. Alonzo, A. d. Schrijver and M. Pagliaro, *Chemical Reviews*, 2011, **111**, 765-789.
45. L. Wu, H. Hu, Y. Xu, S. Jiang, M. Chen, Q. Zhong, D. Yang, Q. Liu, Y. Zhao, B. Sun, Q. Zhang and Y. Yin, *Nano Letters*, 2017, **17**, 5799-5804.
46. Q. A. Akkerman, S. Park, E. Radicchi, F. Nunzi, E. Mosconi, F. De Angelis, R. Brescia, P. Rastogi, M. Prato and L. Manna, *Nano letters*, 2017, **17**, 1924-1930.
47. L. Protesescu, S. Yakunin, M. I. Bodnarchuk, F. Krieg, R. Caputo, C. H. Hendon, R. X. Yang, A. Walsh and M. V. Kovalenko, *Nano Letters*, 2015, **15**, 3692-3696.
48. Q. A. Akkerman, D. Meggiolaro, Z. Dang, F. De Angelis and L. Manna, *ACS Energy Letters*, 2017, **2**, 2183-2186.
49. F. Palazon, F. Di Stasio, Q. A. Akkerman, R. Krahne, M. Prato and L. Manna, *Chemistry of Materials*, 2016, **28**, 2902-2906.